Rational Evaluation and Cycle Life Improvement of Quinone-Based Aqueous Flow Batteries Guided by In-Line Optical Spectrophotometry

David G. Kwabi, Andrew A. Wong,* and Michael J. Aziz **,z

Harvard John A. Paulson School of Engineering and Applied Sciences, Cambridge, Massachusetts 02138, USA

We measure electrolyte concentration and state-of-charge in real time in an operating aqueous anthraquinone-based flow battery using in-line optical spectrophotometry. By capitalizing on the linear transition in absorption spectra between oxidized and reduced states, we show how discontinuous capacity fade rates in redox flow batteries can be caused by a transition from one capacity-limiting electrolyte to the other, which is caused by reactant crossover. With this insight, we demonstrate an electrolyte-balancing scheme, which can be broadly applicable to flow battery systems with asymmetric electrolyte crossover rates.

 [DOI: 10.1149/2.0791809jes]

Manuscript submitted March 23, 2018; revised manuscript received May 22, 2018. Published June 12, 2018.

As the costs of many renewable electricity generation technologies continue to decrease,[1] there is an increasing global interest in potentially inexpensive, safe, and easily deployable energy storage solutions such as redox flow batteries (RFBs).[2–5] Aqueous organic and organometallic flow batteries have become an exciting area of research due to the high earth abundance of their active materials and potentially lower cost than state-of-the-art vanadium-based systems.[6–9] During operation the crossover, decomposition, and side reactions of redox-active species and solvent will change both the state-of-charge (SOC) and concentration of the electrolytes, leading to current inefficiencies and capacity losses.[10] Because of this, active monitoring of electrolyte composition is critical to rationally evaluating and improving battery performance. While electrochemical techniques such as open-circuit voltage[11] and conductivity measurements[12] are useful in this regard, they are also challenging to interpret and sensitive to spurious changes in potential related to impurities, electrode conditioning, and atmospheric contamination.

The aromatic structure of organic molecules such as functionalized quinones not only provides an electronic structure for stable and reversible redox reactions, but also creates a unique absorption fingerprint detectable by optical spectrophotometry. Thus, optical spectrophotometry provides an opportunity to gain direct, real-time insight into flow battery performance.[13] Several all-vanadium flow battery studies have used ultraviolet-visible (UV-Vis) spectrophotometry to monitor the SOC of the V^{II}/V^{III} and V^{IV}/V^{V} redox couples.[14–17] These studies use the absorbance spectra at different SOCs to quantify the well-known 1:1 equilibrium of complex formation between V^{IV} and V^{V} species.[15,16] This demonstrates the unique ability of spectroscopic methods to shed light into speciation during RFB operation. Optical spectrophotometry is becoming an actively used technique for characterizing operating flow battery systems.

Aromatic redox-active organic molecules are particularly interesting candidates for spectrophotometric analysis due to the sensitivity of their electronic structure to π-conjugation,[18] functionalization,[19] and redox state.[20] For RFBs with these active organic electrolytes, optical spectrophotometry is thus a powerful tool for direct, continuous monitoring of battery SOC. The report[6] in 2014 of an aqueous RFB with a 9,10-anthraquinone-2,7-disulfonic acid (AQDS) negative electrolyte (negolyte) against a HBr/Br_2 positive electrolyte (posolyte) triggered a flood of interest in redox-active organics for aqueous RFBs. It has recently been shown that both the SOC and the quinhydrone dimer equilibrium constant with the reduced and oxidized AQDS species can be quantified using UV-Vis spectrophotometry, providing insight into the electrochemical behavior of this electrolyte.[21]

Here we report the use of UV-Vis spectrophotometry to monitor real-time performance of an AQDS-Br^- RFB under different applied potentials, current densities and flow rates. In particular, we show how the negolyte SOC window changes with current density and flow rate, both of which are strongly correlated with mass transport of AQDS to the electrode. Furthermore, this technique sheds light on one of the major challenges remaining toward the practical implementation of the AQDS-Br^- chemistry: an observed discontinuous and accelerating capacity fade during long-term cycling. In this work, we show that the crossover rate of bromine from the posolyte is four orders of magnitude faster than that of AQDS from the negolyte. Prior work has shown discontinuous capacity fade of an AQDS-Br^- cell whose capacity is limited by the negolyte (negolyte-limited) and whose AQDS crossover and decomposition rates are both slow; it has been hypothesized that discontinuous capacity fade is due to bromine crossover from the posolyte to the negolyte, resulting in the posolyte becoming capacity-limiting (posolyte-limited).[22] Optical spectrophotometry illuminates this transition and shows the value of in-line monitoring of quinone-based flow batteries. With this insight, we develop a passive electrolyte balancing scheme by adding HBr to the negolyte, thus creating a $[Br^-]$ gradient driving bromide back toward the posolyte[23] and averting rapid capacity fade caused by loss of the reduced posolyte species. This strategy constitutes a practical, passive method for enabling long-term RFB cycling.

Experimental

The RFB build (Scheme 1a) follows a similar procedure to previous publications.[24–27] The negolyte is composed of 0.3 M AQDS (45 mL) and the posolyte contains 0.8 M HBr (70 mL), both without supporting electrolytes. This is made possible by the strong dissociation of the AQDS sulfonic acid groups as well the HBr electrolyte. All electrochemical cycling experiments are performed using a custom-built flow cell with interdigitated flow channels (Fuel Cell Tech, Albuquerque, NM). Each half-cell electrode consisted of a 3-sheet stack of SGL39AA porous carbon electrodes with 5 cm^2 geometric area baked at 400°C for at least 12 h. The two half-cells are separated by a Nafion 117 (∼175 μm thick) membrane soaked overnight in de-ionized water. Electrolytes are pumped through with a diaphragm pump (Cole Parmer). Variable flow rate experiments are performed with a peristaltic pump (Cole Parmer, MasterFlex L/S) using Teflon tubing to avoid the pulsations of the diaphragm pump. An optical cross flow cell (micro Flow Cell from Custom Sensors & Technology) with adjustable path length is plumbed into the negolyte cell outlet (Scheme 1b). Optical spectrophotometry data were collected through this cross flow cell using a deuterium-tungsten light source (Ocean Optics DH-2000-BAL) and UV-Vis spectrometer (Ocean Optics Flame-S-UV-VIS) connected by a pair of 25 cm optical fibers (Ocean Optics QP400-025-SR-BX).

*Electrochemical Society Student Member.
**Electrochemical Society Member.
zE-mail: maziz@harvard.edu

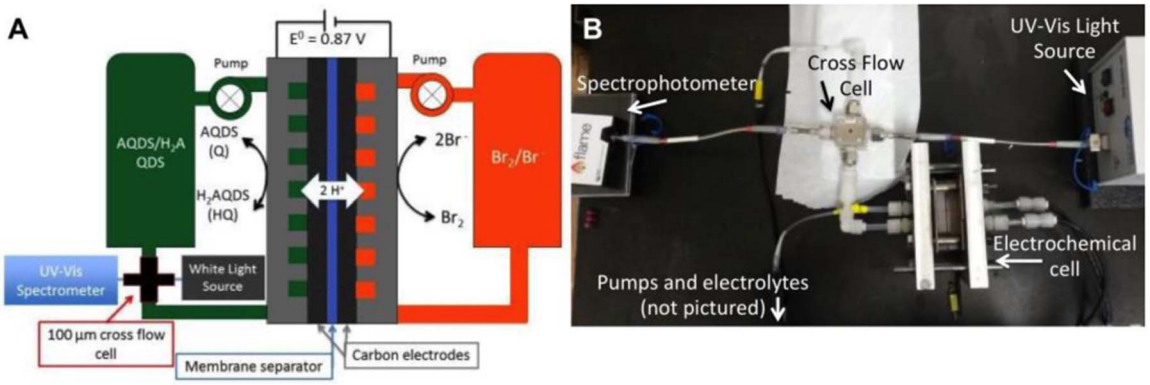

Scheme 1. (a) The optical flow cell full system schematic. (b) Example photograph highlighting the cross flow cell plumbed into the negolyte outlet.

Negolyte spectra at 0% and 100% SOC were established at the ends of a chronoamperometric charge-discharge cycle at 1.3 V and 0.3 V respectively. SOC is defined as the percentage of active AQDS molecules in the reduced form. Intermediate SOC values were determined using linear interpolation between the spectra at 0% and 100% SOC, following the normalization procedure described in previous work.[21] Absorption non-linearities[28] at high concentrations are also discussed by Tong et al.,[21] and instrument non-linearities are considered accounted for in the normalization procedure. To determine the accessible SOC window under different operating conditions, the battery is cycled by constant currents of 0.10, 0.15, 0.20 and 0.25 A/cm^2 all at a 24.4 mL/min flow rate, as well as flow rates of 31.3, 24.4, 16.8, 8.4, 3.4 mL/min all at 0.20 A/cm^2. Each of these variable flow and variable current experiments is conducted well within the time for the posolyte to become capacity-limiting.

To demonstrate the asymmetry in bromine and AQDS crossover rates, the full AQDS-HBr cell, designed to start with negolyte-limited capacity, is cycled at 0.2 A/cm^2 for 79 cycles, during which a precipitous capacity fade is observed. Before the 80th cycle, 35 mL of 0.8 M HBr is added to the posolyte and the capacity is evaluated for subsequent cycles.

In the flux-balanced cell experiment, 2 M HBr is added to the negolyte to balance the flux of bromine atoms between the posolyte and negolyte through the membrane, while 1 M H_2SO_4 is added to the posolyte to balance the electrolyte ionic strengths. Using the same cell hardware as for the asymmetric AQDS-HBr experiment, these new electrolyte solutions are pumped through the cell and also cycled at 0.2 A/cm^2.

Results and Discussion

Initial characterization.—It has been shown[21] that the UV region ($\lambda < 400$ nm) of an AQDS absorbance spectrum at any SOC can be constructed as a linear combination of the (oxidized) quinone and (reduced) hydroquinone (H_2AQDS) spectra. Thus, using negolyte spectra at 0% and 100% SOC as representative of AQDS and H_2AQDS, respectively, we first correlate real-time negolyte SOC to coulombic capacity during galvanostatic charge and discharge steps as shown in Figure 1a. SOC values are obtained by finding the linear combination of AQDS and H_2AQDS that minimized the least-squares error between measured and calculated spectra. As expected, both SOC and capacity increase and decrease monotonically with charge and discharge, respectively, although a lag between SOC and capacity is also observed (see note in SI). These data support the assumption that non-linear absorption behavior is negligible under these conditions.

Figure 1b shows the evolution of the negolyte UV-Vis spectrum from its fully oxidized (AQDS, 0% SOC) to fully reduced (H_2AQDS, 100% SOC) state with an optical path length of ~2 µm. This very short path length enables a non-saturated detection of these high optical density electrolytes. AQDS has absorption peaks at 256 and 331 nm, whereas H_2AQDS has absorption peaks at 270 and 390 nm. In contrast to vanadium systems, where the 1:1 V^{IV}-V^{V} complex absorbs strongly in the UV and obscures absorbance from uncomplexed solution-phase V^{IV} and V^{V} species,[15,17] the 1:1 formation of the quinhydrone complex between AQDS and H_2AQDS does not have this same issue. This is because the quinhydrone only presents a new absorption peak in the visible rather than the UV region.[21] Furthermore, an isosbestic point is observed at 354 nm, which is consistent with interconversion between only two species (i.e. AQDS and H_2AQDS) during charge/discharge, as expected for proton-coupled electron transfer in strongly acidic media.[6,29,30] In contrast, it has been shown[31] that electrochemical AQDS reduction in alkaline media results in the formation of deprotonated and semiquinoid-type species, resulting in no isosbestic points observed in the associated UV-Vis spectra.

Effect of current density and flow rate on accessible negolyte SOC window.—Cycling a RFB potentiostatically enables access to the full negolyte SOC range. However, most RFB cycling studies are conducted galvanostatically, which more closely simulates operation at specified power density inputs or outputs. Voltage cutoffs are used with galvanostatic cycling to prevent undesired side reactions (e.g. water splitting), but due to ohmic resistance and mass transport limits, the full SOC range is inaccessible. Figure 2a shows the maximum SOC attained while charging and the minimum SOC attained while discharging at different current densities for a fixed fluid flow rate (24.4 mL/min). The accessible SOC range, also known as electrolyte utilization, at each current density is 83%, 66%, 48% and 22% for 0.10, 0.15, 0.20 and 0.25 A/cm^2 respectively. The accessible SOC range decreases with increasing current density due to the increasing charge and discharge overpotential with current density. This technique can be used to extrapolate to a maximum achievable current density for a given SOC range at a given fluid flow rate. For example, in this cell configuration, the maximum current density to achieve 80% electrolyte utilization at a flow rate of 24.4 mL/min is approximately 109 mA/cm^2.

Figure 2b demonstrates how the minimum and maximum SOCs for a fixed current density change when varying the fluid flow rate. In an operating flow battery, there is an inherent trade-off between fluid pumping losses and voltage inefficiencies stemming from mass transport losses. Increasing the fluid flow rate decreases the mass transport diffusion layer, but increases the pressure drop through the porous electrode. Because the electrolyte utilization increases with fluid flow rate, this technique can be used to identify a combination of pumping and mass transport parameters that minimizes energy losses for a given RFB system.

Flux-balanced cell scheme.—We now demonstrate that in situ SOC monitoring using UV-Vis spectrophotometry is useful in rationally evaluating capacity fade and extending cycle life in the

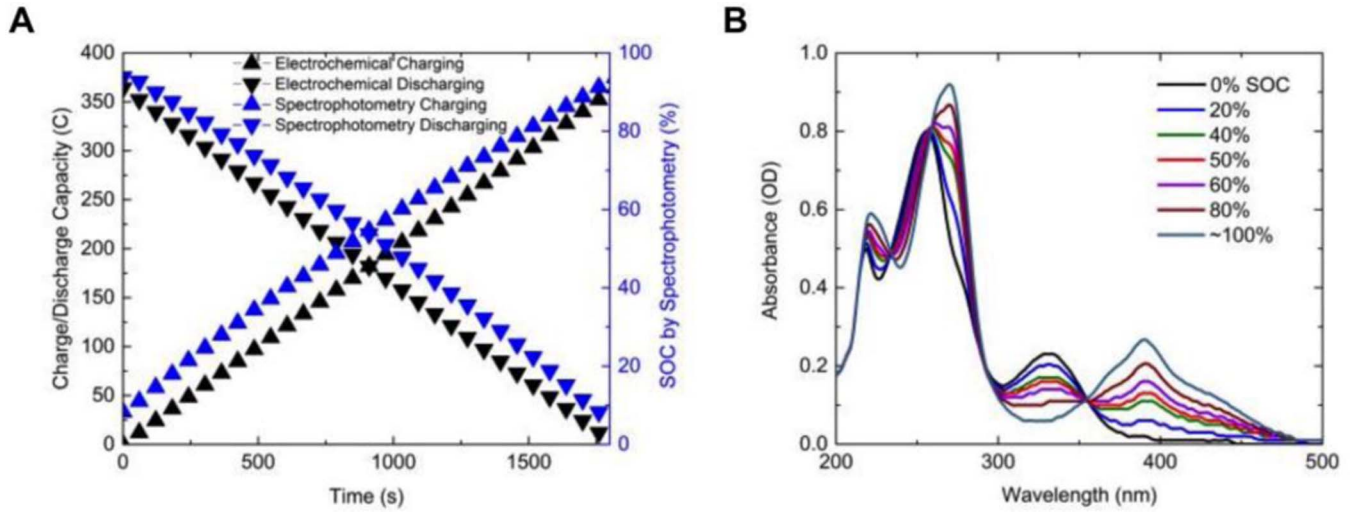

Figure 1. (a) Galvanostatic charge and discharge at 0.20 A/cm^2 showing variation of SOC (monitored by UV-Vis spectrophotometry) and accumulated charge over time. (b) UV-Vis negolyte absorption spectra from 0% SOC to 100% SOC using an in-line spectrometer cross flow cell.

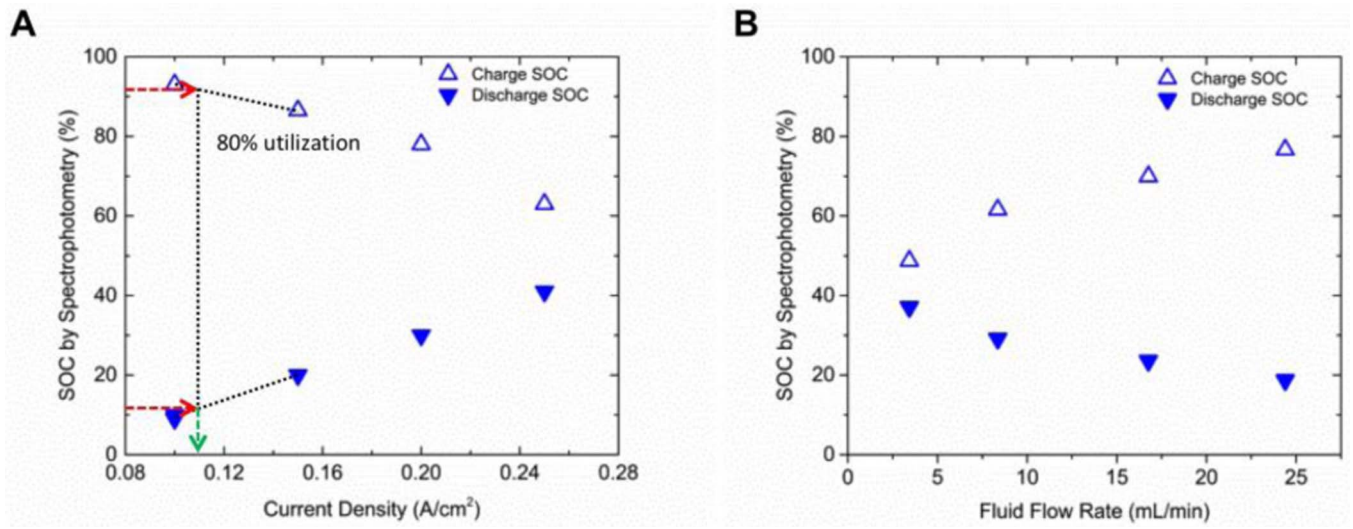

Figure 2. Maximum charge and minimum discharge SOC attained during galvanostatic cycling for (a) changing current densities at 24.2 mL/min fluid flow rate, and (b) changing flow rates at 0.2 A/cm^2. Dashed lines in (a) indicate the operating parameters to achieve 80% negolyte utilization.

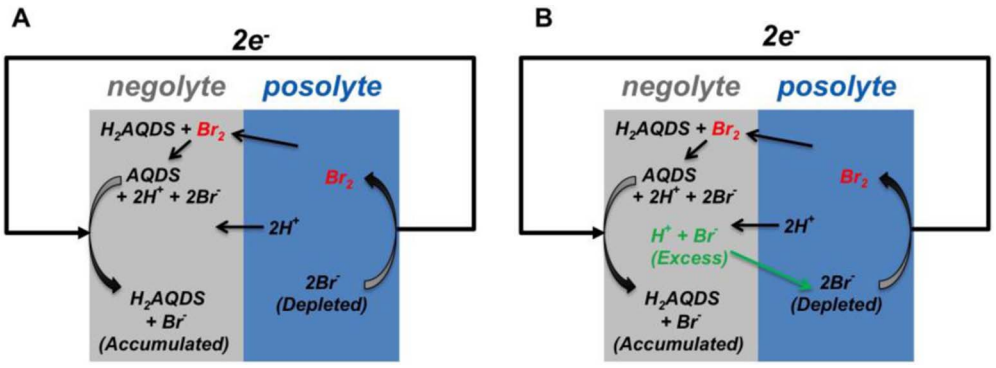

Scheme 2. Scheme showing bromine crossover during AQDS-Br$^-$ cell charging leading to (a) bromine accumulation in the negolyte when Br$^-$ is not present or (b) a counterflux of Br$^-$ ions from the negolyte to replace lost bromine when sufficient HBr is present in the negolyte.

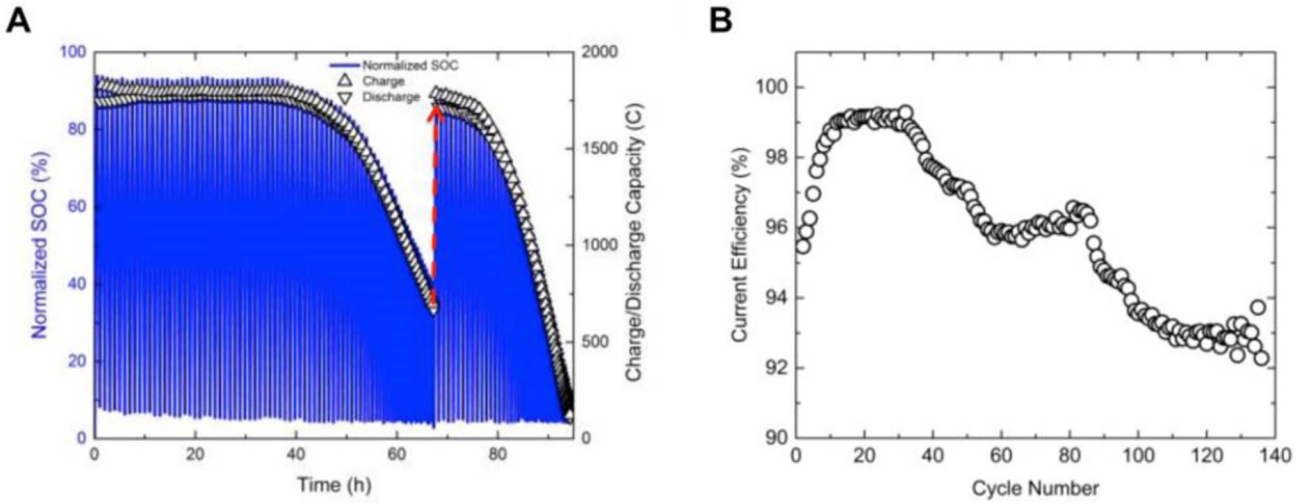

Figure 3. (a) Normalized negolyte SOC and coulombic capacity as functions of time during galvanostatic cycling of a negolyte-limited AQDS-Br^- cell at 0.2 A/cm^2 with a negolyte of 45 mL 0.3 M AQDS and posolyte of 70 mL 0.8 M HBr. The dashed arrow shows where 35 mL of 0.8 M HBr was added to the posolyte. (b) Current efficiency as a function of cycle number for galvanostatic cycling of negolyte-limited cell. The current efficiency drop around cycle 40 corresponds to the capacity fade onset, and the additional drop at cycle 80 corresponds to the HBr addition to the posolyte.

AQDS-Br^- RFB. One of the major remaining challenges toward the practical implementation of AQDS-Br^- chemistry is a suddenly accelerated capacity fade during long-term cycling. It has been recently suggested that this accelerated capacity fade is due to bromine crossover from the posolyte to the negolyte (see Scheme 2a, resulting in the posolyte becoming capacity-limiting.[22] To more fully elucidate this transition, we cycled a negolyte-limited cell with a negolyte of 45 mL of 0.3 M AQDS and posolyte of 70 mL of 0.8 M HBr, while monitoring the SOC of the negolyte. Figure 3a shows the real-time normalized SOC of the negolyte (blue line) and coulombic charge and discharge capacity (black triangles) at the time point corresponding to the end of each half-cycle. After ∼67 hours of galvanostatic cycling at 0.2 A/cm^2, the accessible negolyte capacity window narrows from 8–92% to 8–40%, while the capacity fade rate increases from ∼0.5%/day to ∼50%/day. The strong correlation between a narrowed accessible SOC range and loss of capacity is consistent with a transition of the capacity-limiting side to the posolyte.

To confirm that the posolyte was capacity-limiting, we added 35 mL of 0.8 M HBr (arrow at 67 hours in Figure 3a corresponding to the 80th cycle, resulting in an immediate recovery of the capacity back to its original value around 1800 C; this recovery was followed later by another simultaneous drop in both capacity and accessible SOC range. Further evidence for this transition in capacity-limiting electrolyte can be inferred from plotting capacity and current efficiency as functions of cycle number, as shown in Figure 3b. We attribute the transient increase in current efficiency in the first few cycles to a balancing of negolyte and posolyte SOCs and membrane equilibration in the electrolyte. The average current efficiency during the negolyte-limited cycling regime was 98.5%, This represents an average loss of 1.5% equivalent of negolyte capacity from the posolyte per cycle, and implies that after 72 cycles, the negolyte and posolyte would have equal capacities, after which a sudden drop in capacity would be expected. This transition, which occurs around 40 rather than 72 cycles, can be attributed to mass transport limitations caused by the formation of liquid bromine (i.e. uncomplexed to Br^-), which would be expected to begin after either 26 or 38 cycles, depending on whether or not Br_2 solubility and complexation are taken into account (full calculations in Supporting Information). The dramatic decrease in current efficiency from ∼98% to 92% likewise supports the posolyte becoming capacity-limiting, as molecular bromine is expected to have a higher crossover rate than tribromide (*vide infra*).

We also demonstrate that balancing the flux of bromine to the negolyte with bromide to the posolyte can avoid the accelerated capacity fade observed for the AQDS-Br^- RFB. A first step toward implementing this flux-balanced cell strategy is to estimate the permeabilities of tribromide (Br_3^-, formed by the complexation of bromine, $Br_2 + Br^- \rightarrow Br_3^-$) and bromide through Nafion. To measure tribromide permeability, we constructed a negolyte-limited cell with a negolyte comprising 20 mL of 0.5 M AQDS and 0.5 M H_2SO_4 and a posolyte comprising 20 mL of 3 M HBr, separated by a Nafion 212 membrane.

A thinner style of Nafion separator allows for a higher signal to noise ratio, and therefore more precise measure of membrane permeability, assuming the relative crossover rate of each bromine species is constant. Upon fully charging the cell at 1.3 V, the negolyte was fully reduced and a long-term steady-state current was observed as demonstrated in Figure 4a. This steady-state current of 45 mA results from the formation of a redox shuttle controlled by the flux of tribromide from the posolyte to the negolyte, where it oxidizes H_2AQDS to AQDS, which in turn is continuously re-reduced to H_2AQDS at the carbon electrode (Scheme 2b). This current can be rationalized as due to the flux of tribromide from the posolyte calculated using the equation below:

$$i = nFPA\frac{\Delta c}{t}, \qquad [1]$$

where i is the steady-state current, F is Faraday's constant, P is permeability, A is the geometric area of the electrode, Δc is the difference in concentration between the electrolytes on opposing sides of but immediately adjacent to the membrane, n is number of electrons transferred per molecule of crossing species, and t is membrane thickness. Assuming the steady-state current of 45 mA represents tribromide crossover across a 1 M concentration gradient results in a permeability of 4.6×10^{-7} cm^2/s. This is within an order of magnitude of Br_2 diffusivity through cation-exchange membranes measured using a dialysis cell.[32] We estimated bromide permeability using a similar method, with a posolyte-limited cell composed of a negolyte with 20 mL 0.5 M AQDS and 0.5 M H_2SO_4 and posolyte of 20 mL 0.25 M HBr. Charging the cell at 1.3 V resulted in a similar redox shuttle, whose rate was controlled by the flux of bromide from the negolyte to posolyte, where it was oxidized to bromine. The steady-state current of 165 mA as seen in Figure 4b translates to a bromide permeability of 5.7×10^{-7} cm^2/s.

Given these estimates for bromide and tribromide permeability, we project the concentration of bromide in the negolyte required to balance crossover of tribromide with bromide flux in the opposite

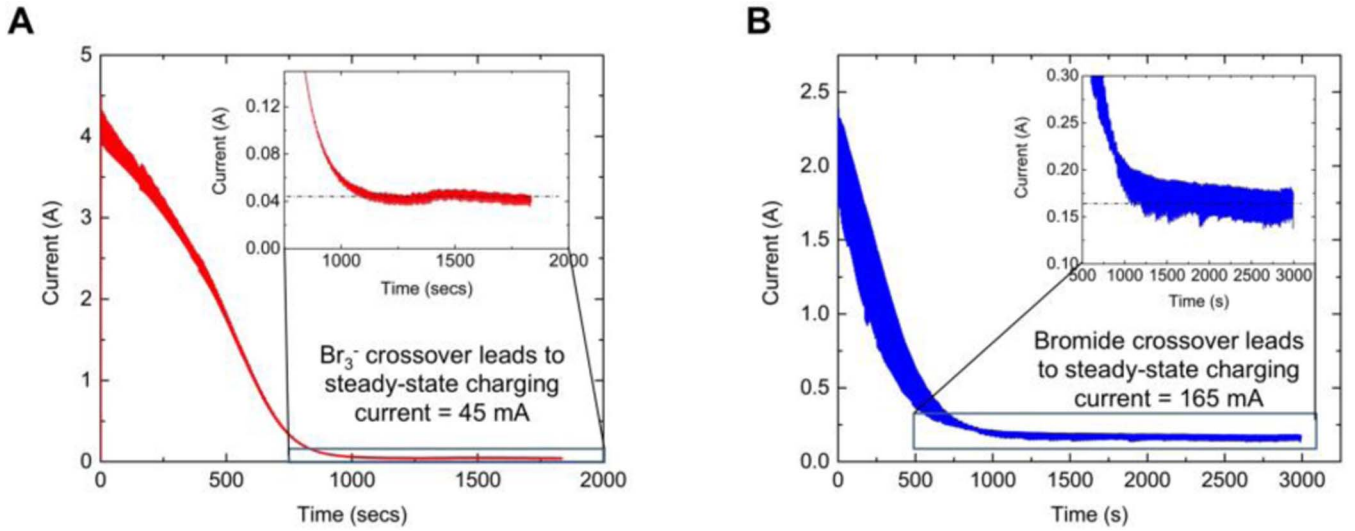

Figure 4. (a) Br_3^- permeability measurement using a cell charged at 1.3 V with a capacity-limiting negolyte of 20 mL 0.5 M AQDS, 0.5 M H_2SO_4 and posolyte of 20 mL 3 M HBr. (b) Br^- permeability measurement using a cell charged at 1.3 V with a capacity-limiting posolyte of 20 mL 0.25 M HBr and negolyte of 20 mL 0.5 M AQDS, 0.5 M H_2SO_4, 3 M HBr.

direction, and avoid the previously observed accelerated capacity fade (Scheme 2b). The result of this analysis is shown in Figure S2 for a capacity-limiting negolyte of 0.3 M AQDS with varying concentrations of Br^-, and a posolyte of 43 mL of 0.8 M HBr. Both tribromide flux from the posolyte to negolyte and bromide flux from the negolyte to posolyte increase as functions of negolyte SOC. In the balanced flux case, tribromide and bromide fluxes (in terms of bromine atoms crossing) are equal at 50% SOC. This occurs for a negolyte with HBr concentration of 0.74 M and is the minimum required negolyte HBr concentration for a flux-balanced RFB; a negolyte with higher Br^- concentration will thus evolve toward a steady-state concentration of 0.74 M during cycling, while one with lower Br^- concentrations will accumulate bromide over time, possibly leading to accelerated capacity fade if the posolyte becomes capacity-limiting. Assuming tribromide and bromide permeabilities scale similarly in cation-exchange membranes, this result will hold true for any membrane thickness and a negolyte HBr concentration of 0.74 M will be sufficient to balance tribromide flux from the posolyte to negolyte with bromide flux from the negolyte to the posolyte.

Over timescales longer than the 2000-second measurement in Figure 4a, however, continuous crossover of tribromide from the posolyte to the negolyte will eventually result in the formation of uncomplexed molecular bromine in the posolyte at high SOCs (see discussion in SI). A higher permeability would be expected for neutrally charged molecular bromine than for negatively charged tribromide ions, as tribromide face coulombic repulsion from negatively charged sulfonate groups in the Nafion membrane whereas bromine do not. As a consequence of the potential contribution of molecular bromine to the flux from posolyte to negolyte, our measured tribromide permeability of 4.6×10^{-7} cm^2/s and consequent minimum required negolyte HBr concentration of 0.74 M represent lower bounds for bromine atom permeability and resulting bromide concentration required for crossover balancing, respectively. In order to counterbalance the potential additional flux due to molecular bromine, a negolyte

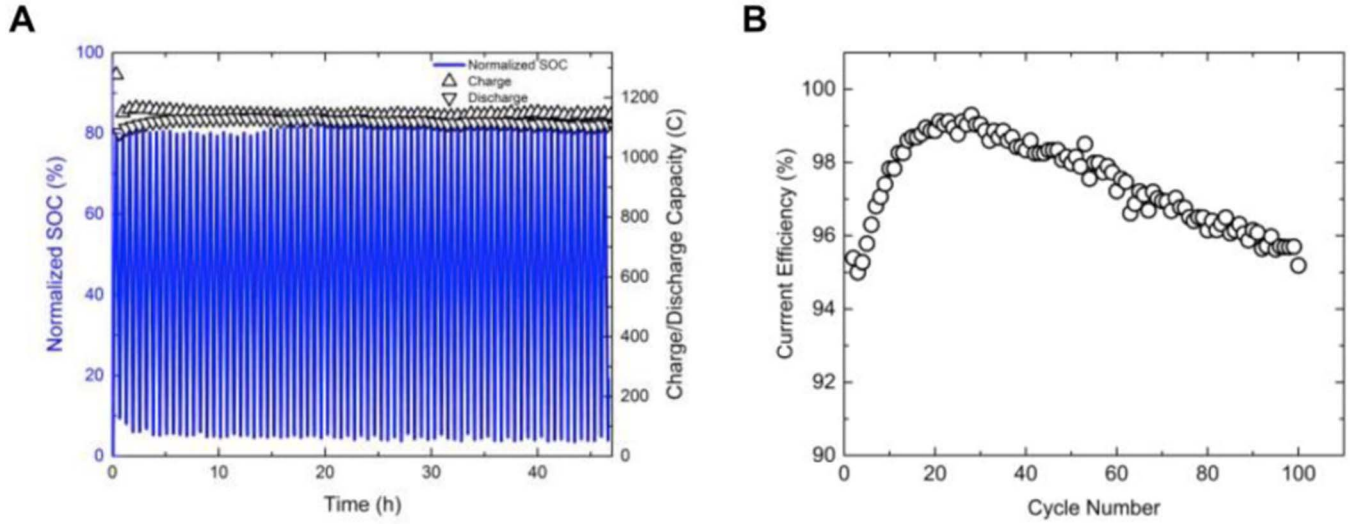

Figure 5. Normalized negolyte SOC and coulombic capacity as functions of time during galvanostatic cycling of a negolyte-limited AQDS-Br^- cell at 0.20 A/cm^2. The negolyte comprises 38 mL 0.3 M AQDS and 2 M HBr and the posolyte comprises 70 mL 0.8 M HBr and 2.7 M H_2SO_4. (b) Current efficiency as a function of cycle number for galvanostatic cycling of the negolyte-limited cell. We attribute the transient increase in current efficiency in the first few cycles to a balancing of negolyte and posolyte SOCs and membrane equilibration in the electrolyte.

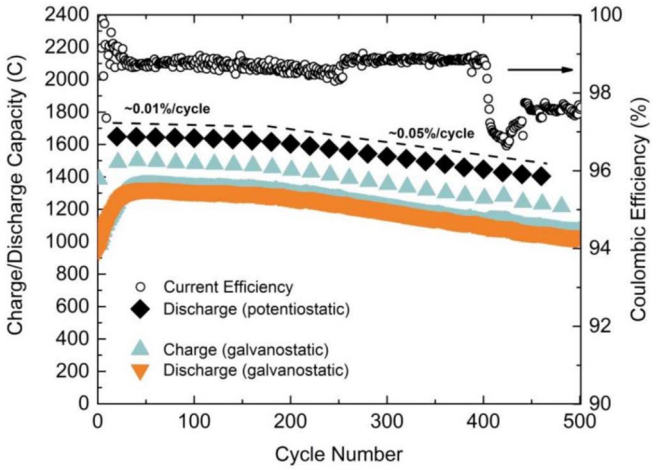

Figure 6. Coulombic capacity and current efficiency vs. cycle number during long-term galvanostatic cycling of flux-balanced cell at 0.2 A/cm^2 between 0.25 and 1.3 V. The negolyte was composed of 35 mL 0.3 M AQDS, 2 M HBr and the posolyte was 43 mL 0.8 M HBr and 2.7 M H_2SO_4. A Nafion N115 membrane was used. Potentiostatic charge-discharge cycles were performed after every 30 galvanostatic cycles, and discharges from those cycles are shown in black diamonds.

HBr concentration of 2 M rather than 0.74 M was used in subsequent experiments.

Coulombic capacity as a function of time using this flux-balanced cell scheme, including negolyte SOC tracked by in situ UV-Vis, is shown in Figure 5. The negolyte is composed of 38 mL of 0.3 M AQDS and 2 M HBr, and the posolyte is composed of 70 mL of 0.8 M HBr and 2.7 M H_2SO_4. For 100 cycles, a steady capacity fade of ∼0.01%/cycle is observed (full cycle data found in Figure S1b, while the current efficiency decays slowly, from 99 to 95% as seen in Figure 5b. In situ UV-Vis measurements of the negolyte also show that the SOC range accessed stays between 5 and 80% SOC for the entire cycling duration; thus, any capacity fade observed is due to either AQDS crossover, leakage, or molecule decomposition.[10,22] The absence of an accelerated capacity fade is consistent with the successful operation of the flux-balanced cell scheme we have described, where bromine crossover is balanced by bromide permeation from the negolyte, preventing the posolyte from becoming capacity-limiting.

We performed a long-term test of the flux-balanced cell configuration to demonstrate the robustness of this concept. Figure 6 shows the performance of a flux-balanced cell cycled 500 times with a capacity-limiting negolyte. Potentiostatic charge-discharge cycles were interspersed after every 30 galvanostatic cycles to assess the true capacity of the cell, i.e. regardless of changes in membrane resistance and mass transport. No precipitous drop in either capacity or current efficiency is observed, in contrast to the unbalanced case shown in Figure 3. There is, however, a change in the capacity fade rate from ∼0.01%/cycle to ∼0.05%/cycle after 200 cycles, the possible origins of which are elaborated upon in the SI. As described in previous work, a time-based capacity fade of a 9,10-anthraquinone-2,7-disulfonic acid negolyte-limited cell is anticipated due to molecular decomposition[22] and could constitute a portion of the observed capacity fade.

Summary

In this work, we report the use of in-line optical absorption spectrophotometry to actively monitor the SOC of an operating AQDS/HBr flow battery; the SOC is used to determine the electrolyte utilization dependence on applied potential, current density and flow rate. We elucidate the value of this technique further by starting the cell as negolyte capacity-limited, and observing steady state charge-discharge behavior of the battery both electrochemically and optically. Eventually, bromine crossover from the posolyte causes the system to become posolyte capacity-limited, leading to a precipitous decrease in the capacity retention rate (∼50%/day). Adding more HBr to the posolyte results in a temporary recovery of that capacity and in corresponding increases in the maximum negolyte charging SOC and electrolyte utilization; this is consistent with the interpretation as a transition of capacity-limiting side. Optical spectrophotometry illuminates these transitions and demonstrates the value of in-line monitoring of quinone-based flow batteries. With this insight, we demonstrate a practical, passive electrolyte balancing method by adding HBr to the negolyte, thus creating a Br^- gradient toward the posolyte and averting rapid capacity fade caused by loss of bromine from the posolyte. Similar balancing schemes may eliminate the need for electrolyte rebalancing for other RFB chemistries with asymmetric electrolyte crossover rates, enabling longer-lasting, high-performance grid-scale energy storage systems.

Acknowledgments

This research was supported partially by the US Department of Energy ARPA-E Award DE-AR0000348, by DE-AC05-76RL01830 through PNNL subcontract 304500, the Harvard School of Engineering and Applied Sciences, and the Massachusetts Clean Energy Center. We thank Dr. Marc-Antoni Goulet for suggesting the crossover measurements in Figure 4, Dr. Michael Gerhardt for useful discussions and Louis Kang for contributing ideas on the system setup.

ORCID

Michael J. Aziz https://orcid.org/0000-0001-9657-9456

References

1. P. Donohoo-Vallett, "Revolution Now 2016 Report_2.Pdf," edited by U.S.D.o. Energy (2016).
2. G. L. Soloveichik, "Flow Batteries: Current Status and Trends," *Chem Rev*, **115**, 11533 (2015).
3. G. L. Soloveichik, "Battery Technologies for Large-Scale Stationary Energy Storage," *Annu Rev Chem Biomol Eng*, **2**, 503 (2011).
4. B. Dunn, H. Kamath, and J. M. Tarascon, "Electrical Energy Storage for the Grid: A Battery of Choices," *Science*, **334**, 928 (2011).
5. M. Skyllas-Kazacos, M. H. Chakrabarti, S. A. Hajimolana, F. S. Mjalli, and M. Saleem, "Progress in Flow Battery Research and Development," *Journal of The Electrochemical Society*, **158**, R55 (2011).
6. B. Huskinson, M. P. Marshak, C. Suh, S. Er, M. R. Gerhardt, C. J. Galvin, X. Chen, A. Aspuru-Guzik, R. G. Gordon, and M. J. Aziz, "A Metal-Free Organic-Inorganic Aqueous Flow Battery," *Nature*, **505**, 195 (2014).
7. K. Lin, Q. Chen, M. R. Gerhardt, L. Tong, S. B. Kim, L. Eisenach, A. W. Valle, D. Hardee, R. G. Gordon, M. J. Aziz, and M. P. Marshak, "Alkaline Quinone Flow Battery," *Science*, **349**, 1529 (2015).
8. S. R. Narayan, G. K. Surya Prakash, B. Yang, L. Hoober-Burkhardt, and S. Krishnamoorthy, "Inexpensive Metal-Free Organic Redox Flow Battery (Orbat) for Grid-Scale Storage," Pat. US 2014/0370403 A1 (2014).
9. T. Janoschka, N. Martin, U. Martin, C. Friebe, S. Morgenstern, H. Hiller, M. D. Hager, and U. S. Schubert, "An Aqueous, Polymer-Based Redox-Flow Battery Using Non-Corrosive, Safe, and Low-Cost Materials," *Nature*, **527**, 78 (2015).
10. Q. Chen, L. Eisenach, and M. J. Aziz, "Cycling Analysis of a Quinone-Bromide Redox Flow Battery," *Journal of The Electrochemical Society*, **163**, A5057 (2016).
11. A. A. Shah, R. Tangirala, R. Singh, R. G. A. Wills, and F. C. Walsh, "A Dynamic Unit Cell Model for the All-Vanadium Flow Battery," *Journal of The Electrochemical Society*, **158**, A671 (2011).
12. M. Skyllas-Kazacos and M. Kazacos, "State of Charge Monitoring Methods for Vanadium Redox Flow Battery Control," *Journal of Power Sources*, **196**, 8822 (2011).
13. P. A. Flowers, M. A. Maynor, and D. E. Owens, "Easily Constructed Spectroelectrochemical Cell for Batch and Flow Injection Analyses," *Analytical Chemistry*, **74**, 720 (2002).
14. W. Zhang, L. Liu, and L. Liu, "An on-Line Spectroscopic Monitoring System for the Electrolytes in Vanadium Redox Flow Batteries," *RSC Advances*, **5**, 100235 (2015).
15. D. N. Buckley, X. Gao, R. P. Lynch, N. Quill, and M. J. Leahy, "Towards Optical Monitoring of Vanadium Redox Flow Batteries (Vrfbs): An Investigation of the Underlying Spectroscopy," *Journal of the Electrochemical Society*, **161**, A542 (2014).
16. C. Petchsingh, N. Quill, J. T. Joyce, D. N. Eidhin, D. Oboroceanu, C. Lenihan, X. Gao, R. P. Lynch, and D. N. Buckley, "Spectroscopic Measurement of State of Charge in Vanadium Flow Batteries with an Analytical Model of V(Iv)-V(V) Absorbance," *Journal of the Electrochemical Society*, **163**, A5068 (2016).
17. Z. Tang, D. Aaron, A. B. Papandrew, and T. A. Zawodzinski Jr, "Monitoring the State of Charge of Operating Vanadium Redox Flow Batteries," *ECS Transactions*, **41**, 1 (2012).

18. R. S. Sanchez-Carrera, M. C. R. Delgado, C. Ferron, R. M. Osuna, V. Hernandez, J. T. L. Navarrete, and A. Aspuru-Guzik, "Optical Absorption and Emission Properties of End-Capped Oligothienoacenes: A Joint Theoretical and Experimental Study," *Organic Electronics*, **11**, 1701 (2010).
19. M. T. Huynh, C. W. Anson, A. C. Cavell, S. S. Stahl, and S. Hammes-Schiffer, "Quinone 1 e- and 2 e-/2 H+ Reduction Potentials: Identification and Analysis of Deviations from Systematic Scaling Relationships," *J Am Chem Soc*, **138**, 15903 (2016).
20. S. Das, A. Bhattacharya, P. C. Mandal, M. C. Rath, and T. Mukherjee, "One-Electron Reduction of 1,2-Dihydroxy-9,10-Anthraquinone and Some of Its Transition Metal Complexes in Aqueous Solution and in Aqueous Isopropanol-Acetone-Mixed Solvent: A Steady-State and Pulse Radiolysis Study," *Radiation Physics and Chemistry*, **65**, 93 (2002).
21. L. Tong, Q. Chen, A. A. Wong, R. Gomez-Bombarelli, A. Aspuru-Guzik, R. G. Gordon, and M. J. Aziz, "Uv-Vis Spectrophotometry of Quinone Flow Battery Electrolyte for in-Situ Monitoring and Improved Electrochemical Modeling of Potential and Quinhydrone Formation," *Phys. Chem. Chem. Phys.*, **19**, 31684 (2017).
22. M. R. Gerhardt, E. S. Beh, L. Tong, R. G. Gordon, and M. J. Aziz, "Comparison of Capacity Retention Rates During Cycling of Quinone-Bromide Flow Batteries," *MRS Advances*, 1 (2016).
23. R. Darling, K. Gallagher, W. Xie, L. Su, and F. Brushett, "Transport Property Requirements for Flow Battery Separators," *Journal of The Electrochemical Society*, **163**, A5029 (2015).
24. Q. Chen, L. Eisenach, and M. J. Aziz, "Cycling Analysis of a Quinone-Bromide Redox Flow Battery," *Journal of The Electrochemical Society*, **163**, A5057 (2015).
25. Q. Chen, M. R. Gerhardt, and M. J. Aziz, "Dissection of the Voltage Losses of an Acidic Quinone Redox Flow Battery," *Journal of The Electrochemical Society*, **164**, A1126 (2017).
26. Q. Chen, M. R. Gerhardt, L. Hartle, and M. J. Aziz, "A Quinone-Bromide Flow Battery with 1 W/Cm2 Power Density," *Journal of the Electrochemical Society*, **163**, A5010 (2015).
27. M. R. Gerhardt, L. Tong, R. Gomez-Bombarelli, Q. Chen, M. P. Marshak, C. J. Galvin, A. Aspuru-Guzik, R. G. Gordon, and M. J. Aziz, "Anthraquinone Derivatives in Aqueous Flow Batteries," *Advanced Energy Materials*, 1601488 (2017).
28. J. F. Offersgaard and H. Ojelund, "Correction of Nonlinear Effects in Absorbance Measurements," *Applied Spectroscopy*, **56**, 469 (2002).
29. E. Laviron, "Electrochemical Reactions with Protonations at Equilibrium Part Xii. The 2e-, 2h+ Homogeneous Isotopic Electron Exchange Reaction (Nine-Member Square Scheme)," *Journal of Electroanalytical Chemistry*, **169**, 29 (1984).
30. M. Quan, D. Sanchez, M. F. Wasylkiw, and D. K. Smith, "Voltammetry of Quinones in Unbuffered Aqueous Solution: Reassessing the Roles of Proton Transfer and Hydrogen Bonding in the Aqueous Electrochemistry of Quinones," *Journal of American Chemical Society*, **129**, 12847 (2007).
31. G. H. Kelsall and I. Thompson, "Redox Chemistry of H2s Oxidation by the British Gas Stretford Process Part Iii: Electrochemical Behavior of Anthraquinone 2,7 Disulphonate in Alkaline Electrolytes," *Journal of Applied Electrochemistry*, **23**, 296 (1993).
32. A. Heintz and C. Illenberger, "Diffusion Coefficients of Br2 in Cation Exchange Membranes," *Journal of Membrane Science*, **113**, 175 (1996).

SUPPORTING INFORMATION

Rational Evaluation and Cycle Life Improvement of Quinone-Based Aqueous Flow Batteries Guided by In-Line Optical Spectrophotometry

David G. Kwabi, Andrew A. Wong, Michael J. Aziz

Note on lag between coulombic capacity and SOC in Figure 1(a).

A time lag is observed between coulombic capacity and SOC in **Figure 1**(a). This can be attributed to two causes: First, whereas the spectroscopy SOC scale is aligned such that it starts at 0% SOC (fully oxidized AQDS) and ends at 100% SOC (fully reduced H_2AQDS), the coulometry scaling is arbitrary, because the zero point is not necessarily consistent with fully oxidized AQDS. Second, there is a temporal delay between charging the electrolyte and measuring its SOC at the spectrometer. This is due both to the physical movement of fluid from the cell to the spectrometer (about 6 inches), and the fact that there is uneven mixing of instantaneously charged/discharged AQDS with the rest of the electrolyte, resulting in the fluid that exits the cell always at a higher (on charge) or lower (on discharge) then the fluid flowing in.

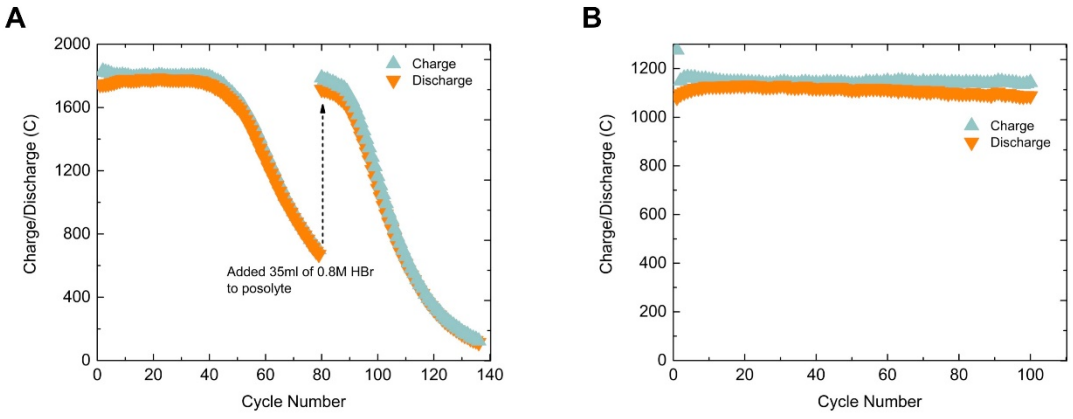

Figure S1. Coulombic capacity as a function of cycle number for galvanostatic cycling of negolyte-limited (a) unbalanced cell shown in **Figure 3** and (b) flux-balanced cell shown in **Figure 3**.

Estimation of required number of cycles for switch in limiting electrolyte.

The average current efficiency for the first 40 cycles is 98.5%.

Assuming this is caused by bromine crossover amounting to 1.5% of the negolyte capacity every cycle, we calculate how many cycles would be required for the initially negolyte-limited cell described in **Figure 3** to become posolyte-limiting. This would occur when

$$\frac{1.5\%}{cycle} \times 45ml \times 2 \times 0.3M \times 96{,}485 \frac{coulomb}{mol} \times \#cycles = \left((0.8M \times 70\,ml) - (0.3M \times 2 \times 45ml)\right) \times 96{,}485 \frac{coulomb}{mol}$$

where the negolyte consists of 45 mL of 0.3 M AQDS (2 e^-/mol) and the posolyte consists of 70 mL of 0.8 M HBr. Solving for number of cycles yields 72 as the transition point. Assuming that the species crossing over is not molecular bromine but a bromine-bromide complex, we use this result to estimate the average number of bromide ions that would need to be coupled to each neutral bromine atom in order for the cell to switch capacity-limiting sides after 40 cycles. Since the calculation above assumes no bromide crossover and results in a transition at 72 cycles, a transition at 40 cycles would require (72/40 – 1) ~ 0.8 Br^- ions crossing over for every neutral bromine atom. This is higher than that for tribromide (0.5, i.e. 1 Br^- for every 2 Br atoms) or pentabromide (0.25, 1 Br^- for every 4 Br atoms). Uncomplexed molecular bromine is therefore expected to comprise a significant fraction of species crossing over from the posolyte.

Because liquid bromine is both more volatile and ~3× more dense than aqueous HBr, it may evaporate and/or phase-separate into areas of the cell architecture and plumbing that cannot be circulated into the electrode manifold. This will reduce the accessible posolyte capacity and cause the posolyte to become capacity-limiting before 72 cycles. To a first approximation, undissolved liquid bromine would start to exist at posolyte SOCs greater than 2/3, beyond the point where molecular bromine is fully complexed into tribromide, $Br_2 + Br^- \rightarrow Br_3^-$:

$$\frac{1.5\%}{cycle} \times 45ml \times 2 \times 0.3M \times 96{,}485 \frac{coulomb}{mol} \times \#cycles = \left((0.8M \times 70ml) - 1.5 \times (45ml \times 2 \times 0.3M)\right) \times 96{,}485 \frac{coulomb}{mol}$$

where the additional factor of 1.5 comes from the inverse of the 2/3 SOC stated above. Solving for number of cycles in this case yields 38 cycles as the point where liquid bromine begins to be produced in the cell.

Given, however, that bromine has a small, but non-zero solubility in water (4 mM), and an equilibrium constant of complexation, *K*, with bromide of about 16.85 M^{-1}[1], we may obtain a more thorough estimate by taking both properties into account:

$$K = \frac{[Br_3^-]}{[Br_2][Br^-]}$$

$$2[Br_2] + [Br^-] + 3[Br_3^-] = T$$

where T is the total bromine atom concentration of 0.8 M. Solving for [Br^-] at the Br_2 solubility limit of 4 mM yields a Br^- concentration of 0.65 M, as the transition point for the accumulation of undissolved bromine. Using this assumption, we can rearrange the equation to account for the number of cycles required to reach a posolyte Br^- concentration of 0.65 M, after which Br_2 would be insoluble:

$$\frac{1.5\%}{cycle} \times 45ml \times 2 \times 0.3M \times 96{,}485 \frac{coulomb}{mol} \times \#cycles = \left((0.8M \times 70ml) - (0.65M \times 70ml)\right) \times 96{,}485 \frac{coulomb}{mol}$$

Solving for the number of cycles before passing the Br_2 solubility limit yields 26 cycles. Given that bromine solubility may vary with pH, we also calculated the number of cycles required for the capacity-limiting side transition assuming Br_2 solubilities of 2 and 8 mM, which yielded 14 and 42 cycles respectively. This shows that this approximation is sensitive to the initial assumptions about Br_2 solubility in aqueous solutions. The 42 cycle estimate (assuming 8 mM Br_2 solubility) is closer to the experimental result (~40 cycles) than the 26 cycle estimate (assuming 4 mM Br_2 solubility); this suggests that Br_2 solubility is higher than 4 mM in acidic aqueous solutions.

Additional details regarding permeabilities to Br_3^-/Br^- and flux-balanced cell.

Tribromide and bromide permeabilities through Nafion 212 were measured *in situ* in a cell with flowing electrolytes rather than *ex situ*, in order to construct a more realistic model for their fluxes across the membrane in a full cell. The cell build was similar to that described in the Experimental Section and Scheme 1(a), but with no UV-Vis cross flow cell. Negolyte- and posolyte-limited cell compositions were used to probe steady-state tribromide and bromide fluxes, as represented by the relevant steady-state currents. As shown in the main text, the current can be rationalized as due to species flux from the equation below:

$$i = nFPA\frac{\Delta c}{t},$$

where i is the steady-state current, F is Faraday's constant, P is permeability, A is the geometric area of the electrode, Δc is the difference in concentration between the electrolytes on opposing sides of but immediately adjacent to the membrane, n is number of electrons transferred per molecule of crossing species, and t is membrane thickness. Permeabilities obtained using this method were then used to calculate Br^- and Br flux from the negolyte to posolyte and *vice versa*, respectively, as a function of SOC. Here, the flux was simply calculated as $P\frac{\Delta c}{t}$, where Δc varies with SOC based on the capacity difference between the negolyte and posolyte.

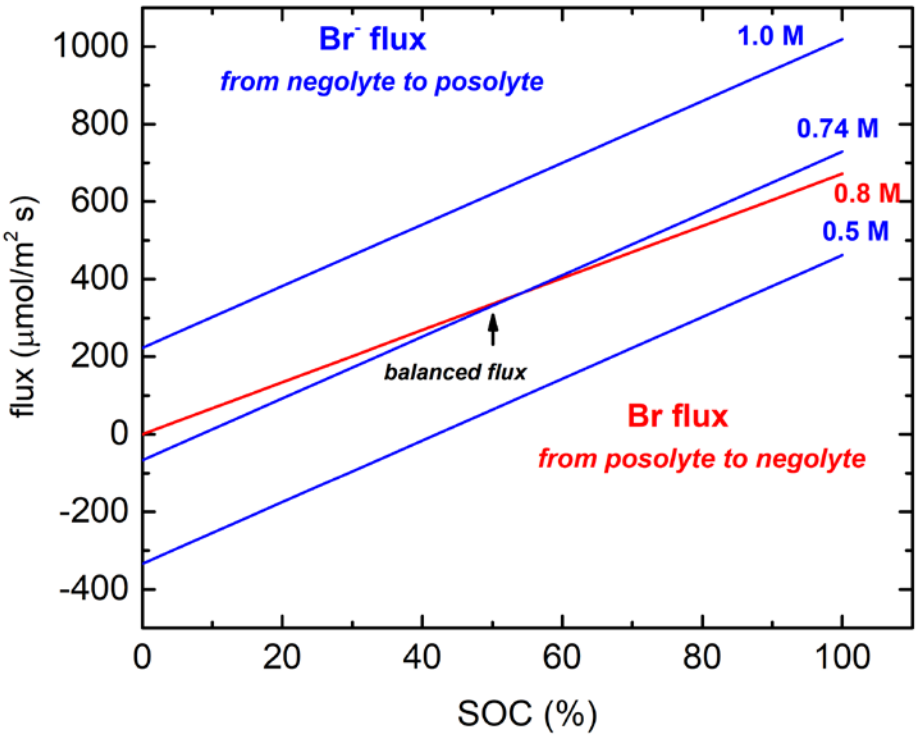

Figure S2. Calculated fluxes of Br^0 and Br^- from posolyte to negolyte and negolyte to posolyte, respectively, as a function of negolyte SOC and HBr concentration, assuming a negolyte of 35 mL 0.3M AQDS and posolyte of 43 mL 0.8M HBr. Different negolyte HBr concentrations are indicated in blue, whereas the starting posolyte HBr concentration is shown in red.

Extended Cycling Experiment

In order to ascertain whether the drop in coulombic efficiency for the 500-cycle flux-balanced cell is due to a change in capacity-limiting electrolyte, we examine total AQDS and Br^- concentration in the negolyte using a combination of UV-Vis spectrophotometry and cyclic voltammetry (CV) after 100 cycles of a similar galvanostatic test (Figure S3). Separate UV-Vis measurements of neat AQDS solution and AQDS with HBr show that at wavelengths above 250 nm, the influence of HBr on the AQDS spectrum is negligible (Figure S4). Two sets of peaks are observed in the CV measurements: the set centered around 0 mV *vs* Ag/AgCl (0.2 V *vs* SHE) corresponds to the AQDS redox process [2], whereas the higher potential pair represents Br_2/Br^-. Both UV-Vis and CV are in agreement in showing that there is negligible change in total AQDS concentration after cycling, as shown by measurements of AQDS concentration in the cycled and uncycled negolytes quantified using a calibration curve, and the similarity in CV peaks, respectively. A comparison of the Br_2/ Br^- redox peaks, however, clearly shows a *reduction* in peak redox

currents, which is consistent with a reduction in negolyte bromide concentration after cycling, and thus, net transfer of bromide from the negolyte to the posolyte and not *vice versa* as would be the case for an unbalanced cell where the posolyte had become capacity-limiting.

The accelerated capacity fade observed in Figure 6 must therefore be due to some cause other than AQDS decomposition or bromine crossover from the posolyte. Side reactions cannot account for the observed behavior, as they would result only in a coulombic efficiency loss, rather than capacity fade [3]. An examination of the cycled electrolytes after a full potentiostatic discharge (**Figure S5**(a)) furnishes a hypothesis. While the cycled negolyte retains the same amber color as the uncycled, characteristic of AQDS at 0% SOC, the cycled posolyte is red in color, and clearly at a higher SOC than its transparent uncycled counterpart, due to the presence of liquid bromine [4]. We therefore hypothesize that during cycling, oxidation of bromide (which is in excess of AQDS capacity by a factor of 1.5) at the posolyte is balanced by a significant amount of reductive charge from the reduction of AQDS formed from O_2 oxidation of H_2AQDS, hydrogen evolution, or other parasitic reactions. This would result in a slow increase in the posolyte SOC over time (**Figure S5**(b)), until the range of accessible capacity cannot match the SOC range of the negolyte, leading to capacity fade. We hypothesize that SOC imbalance between the electrolytes is perpetuated by phase-separation of bromine into "dead" zones/regions of the cell plumbing that cannot be circulated into the electrode manifold to be reduced back to bromide, or volatilization into the gas phase (a progressive reddening of the posolyte reservoir head space was observed during cycling). Further investigation both into ways of engineering more homogenous dispersion of liquid bromine in flow cells, or preventing side reactions caused by O_2 in air may go a long way toward more fully enabling balanced and long-lived AQDS-Br^- cells with long lifetimes, or similar RFB technologies with asymmetric crossover rates of active electrolyte species.

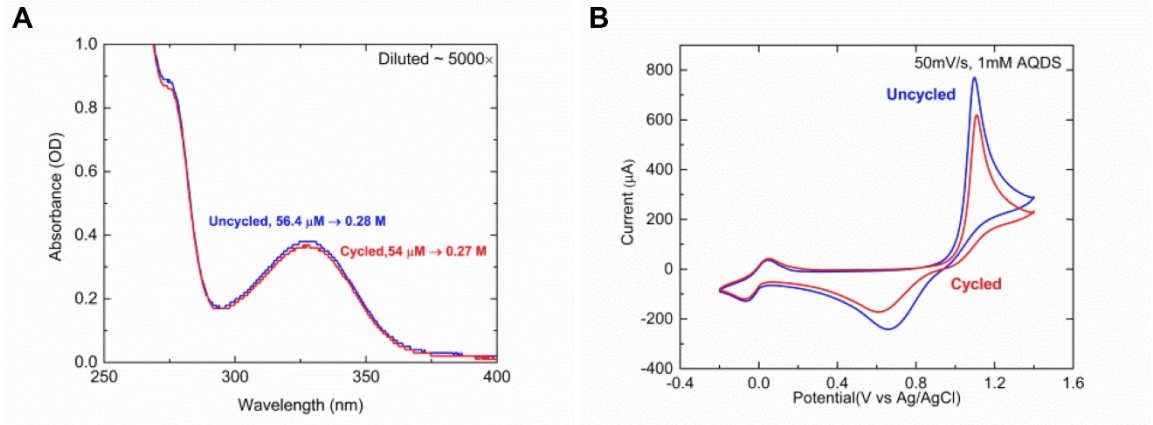

Figure S3. (a) UV-Vis spectra through a 1 cm path length cuvette and (b) cyclic voltammetry analysis of cycled and uncycled negolytes from flux-balanced cell. Negolytes were diluted down to 60 µM and 1mM respectively.

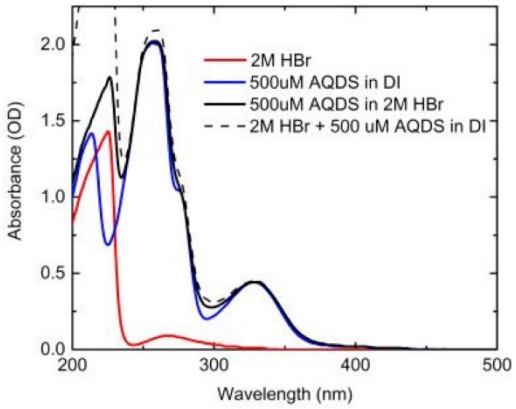

Figure S4. UV-Vis spectra of various solutions through a 1 mm path length cuvette, highlighting the minimal influence of high HBr concentration on the AQDS spectra. The red line is the absorbance spectrum of 2 M HBr showing its significant absorbance peak below 250 nm. The blue line is 500 µM AQDS in deionized water, which varies only slightly from 500 µM AQDS in 2 M HBr (black line). The dashed black line is the sum of the 2 M HBr absorbance (red) and 500 µM AQDS (blue) showing the minimal solvent effect on the absorbance spectra when AQDS is in 2 M HBr. Absorbance optical density > 2 is considered at the signal to noise limitation of the detector.

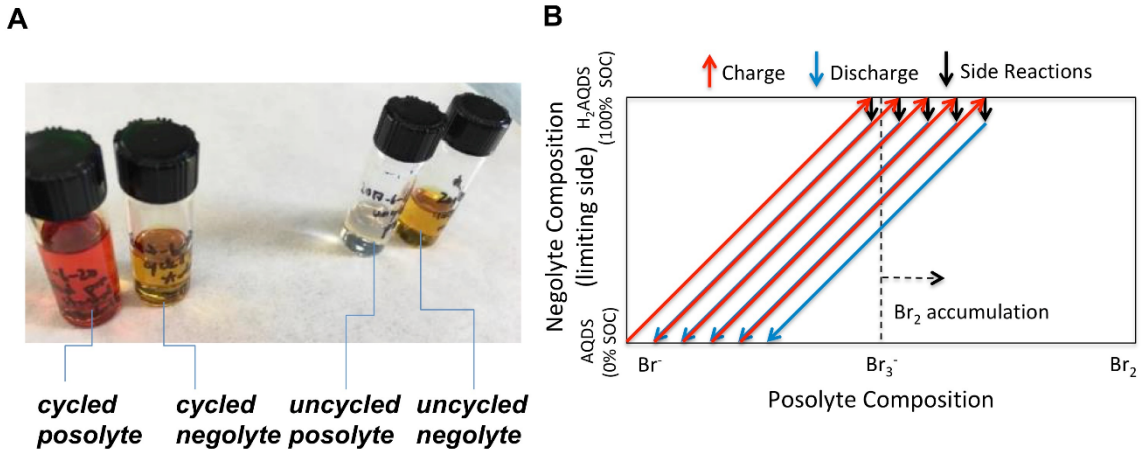

Figure S5. (a) Images of cycled and uncycled electrolytes (b) Schematic illustrating hypothesis that increasing posolyte SOC due to buildup of bromine results in loss of accessible capacity to match SOC range of the negolyte. X- and Y-axes are scaled to the initial relative AQDS:HBr ratio.

[1]D.B. Scaife and H.J.V. Tyrrell, "Equilibrium Constants for the Reaction between Bromine and Bromide at 5, 25 and 35 Degrees in Aqueous Medium of Constant Ionic Strength and Acidity", *J. Chem. Soc.* 386 (1958).

[2]B. Huskinson, M.P. Marshak, C. Suh, S. Er, M.R. Gerhardt, C.J. Galvin, X. Chen, A. Aspuru-Guzik, R.G. Gordon, and M.J. Aziz, "A Metal-Free Organic-Inorganic Aqueous Flow Battery", *Nature* **505**, 195 (2014).

[3]Q. Chen, L. Eisenach, and M.J. Aziz, "Cycling Analysis of a Quinone-Bromide Redox Flow Battery", *Journal of The Electrochemical Society* **163**, A5057 (2016).

[4]S. Biswas, A. Senju, R. Mohr, T. Hodson, N. Karthikeyan, K.W. Knehr, A.G. Hsieh, X. Yang, B.E. Koel, and D.A. Steingart, "Minimal Architecture Zinc–Bromine Battery for Low Cost Electrochemical Energy Storage", *Energy Environ. Sci.* **10**, 114 (2017).